Flow-based pultrusion of continuous fibers for cement-based composite material and additive manufacturing: rheological and technological requirements

Léo Demont, Nicolas Ducoulombier, Romain Mesnil, Jean-François Caron

Flow-Based Pultrusion of continuous fibers for cement-based composite material and additive manufacturing: rheological and technological requirements

Léo Demont[a], Nicolas Ducoulombier[a], Romain Mesnil[b], Jean-François Caron *[a],

[a] *Navier Laboratory, École des Ponts ParisTech, Univ. Gustave Eiffel, CNRS, Marne-La-Vallée, France*
[b] *École des Ponts ParisTech, Marne-La-Vallée, France*

Abstract

The vast majority of applications of extrusion-based concrete additive manufacturing deal with unreinforced mortar. The lack of reinforcement is a serious limitation for the industrial development of 3d printed concrete, because of the brittleness and lack of tensile strength of unreinforced mortar. In this paper, a new reinforcement method inspired by pultruded composite manufacturing, called flow-based pultrusion (FBP), is described and used. The principle is that continuous fiber rovings are impregnated and pulled by the matrix flow, avoiding motorisation, and increasing the apparent yield stress of the mortar and consequently its usability. The hardened resulting material, called *anisotropic concrete*, is unidirectionally and homogenously reinforced. For such composite material, the reinforcement ratio is an important material parameter that relates to specific process variables: roving type, roving count, and output diameter. This article further investigates the effect of the percentage of reinforcement on the process. It also highlights technical requirements to provide the first specifications for flow-based pultrusion.

Keywords: additive manufacturing, concrete, composite materials, yield

*Corresponding author
E-mail: jean-francois.caron@enpc.fr

stress, pressure drop, shear transfer

1. Concrete 3D printing, reinforcement strategies and flow-based pultrusion proposal

Cement-based materials such as concrete and mortars are widely used in the construction industry thanks to their durability and affordability. Due to low tensile properties, they are mostly reinforced with traction-resistant materials to produce structures with suitable mechanical behaviour, i.e. good flexural resistance and ductility.

A particular aspect of the construction industry is that specifications and constraints are highly variable, which finally makes many buildings, infrastructures, and other constructions unique pieces. Traditional concrete manufacturing methods evolved with this variability in mind to produce custom-made structures with various ways of reinforcement. The most common approach is the on-site casting of concrete into a formwork, where rebars are placed to reinforce the hardened concrete. This flexible process allows a great variety of shapes and is scalable from small houses to stadia. However, formwork manufacturing and rebar assembly mainly rely on human labour.

Digital concrete manufacturing holds the promise to address this need for variability with the benefits of automation, especially increased productivity and reduced fabrication tolerance. Within this field, 3D printing based on material extrusion has emerged as an attractive idea to fabricate not only bespoke but also more efficient structures. Indeed, the principle of material shaping by deposition of layers opens a large geometric design space, allowing for simple or complex surfaces alike without added cost. This can be leveraged to reduce material use compared to casting, which is more adapted to simple volumes as the formwork cost grows with complexity. 3D printing makes formwork unnecessary, and optimizes material use thanks to the formal freedom provided by the process.

In practice, 3d printing is more commonly achieved by robotic extrusion pro-

cesses. They consist of the pumping and layer-wise deposition of a yield stress fluid, such as concrete, by a robotic manipulator. However, extruded concrete has mainly remained unreinforced so far, and is thus not adapted to most classical applications. This is a key issue for the industrial development of these technologies. Various approaches, recently reviewed in [1], have been proposed to address this challenge: from post-reinforcement of the printed parts with steel rebars [2] to post-tensioned cables [3].

Process engineering and design of hybrid co-extruders also led to innovative proposals at the extrusion scale, e.g. unrolling of a cable [4] or a wire mesh [5] within the extruded concrete, allowing for reinforcement continuity. In [6] a recent development is proposed and consists on the deposition in the printed lace, of a MCF (Mineral-impregnated Carbon-Fiber) roving, obtained from a continuous, stationary impregnation line. For now, these approaches are limited to low reinforcement amounts. On one hand, one could use heavier cables or meshes, but as their thickness is already about 1mm, bending stiffness becomes significant and limits the printed lace curvature, which makes it difficult to achieve turns while printing. Moreover, it would certainly yield poor interfacial strength between reinforcement and mortar because of the lower specific surface area of the reinforcement. On the other hand, one could multiply reinforcement items distributed over the lace section, but at the cost of complexity of the process control: indeed, in the case of a curved path the unrolling of the inside bend reinforcement must be properly driven to have a lower deposition speed than the outside bend one. However, a good distribution of smaller diameter reinforcement items increases their specific surface area, which leads to a better reinforcement efficiency thanks to an improved anchorage with concrete.

Finally, material science knowledge helps to design reinforcements at the material scale, in line with existing *Ultra High-Performance Fiber Reinforced Concrete* (UHPFRC) or shotcrete applications. In this area, numerous efforts have been made to study the effects of adding short fibers in concrete at the mixing stage. At hardened state, tensile stresses are transferred to fibers which can provide very good post-cracking behaviour and improved tensile behaviour

[7, 8]. However, fibers remain short, and reinforcement rates over 3% appears difficult to achieve as increased fiber amounts alters material pumpability, which is a requirement for robotic extrusion. This is comparable to the usual reinforcement ratio with steel rebars, but such reinforcement is generally aligned with tensile stresses.

In this work, a new method for 3D print continuously reinforced concrete, called *flow-based pultrusion* for additive manufacturing(FBP), is described and used. Inspired by pultruded composite manufacturing, it is however very different. As for pultrusion, it consists of adding numerous very small continuous fiber rovings well-distributed in the lace section. It represents already something totally new for concrete at this scale (less than 1mm diameter rovings) to our knowledge. Moreover and this point is crucial, here no motorization but just the concrete flow to pull on the rovings. It is only possible thanks to the very specific behavior of the fresh concrete, a non-newtonian fluid. Its evolving yield-stress during extrusion permits to be sufficiently fluid for a good impregnation of the introduced fibers, and to be sufficiently stiff downstream to pull them in the lace. In the context of fused-deposition of polymers by 3D printing, a fused thermoplastic is used in [9] to pull long carbon fibers, but the material principle, the scale and the applications are quite different. Another novelty of the present proposal is that the resulting cement-based composite material, called *anisotropic concrete*, is homogeneously reinforced with well-distributed very small rovings along preferred direction. Mechanical tests on casted material specimens (figure 1) shows that such fiber addition can provide ductile, strain-hardening behavior even with low reinforcement ratios of 1%, which is promising.

For such composite material, reinforcement ratio is an important parameter linked with mechanical properties. It is controlled by specific process parameters : roving type, roving count, and output diameter. With the perspective of improving mechanical properties, what is at stake is to understand how reinforcement ratio is limited by process and technological constraints, and one

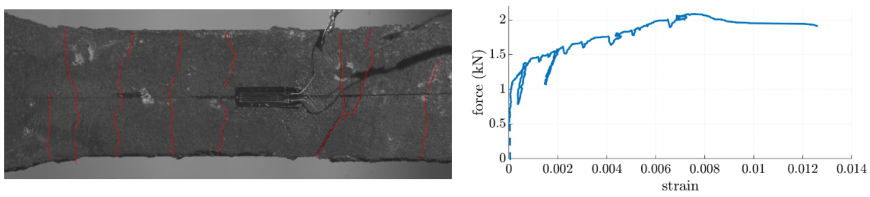

Figure 1: Direct tension test of anisotropic concrete specimen: Video capture of the test specimen at ultimate state showing multiple cracks highlighted in red, Force-strain graph depicting strain-hardening behaviour. Curve jumps are linked with cracking phenomena (from [10]).

may ask what could be the maximal reinforcement ratio. In this paper, the effect of increasing reinforcement ratio on process and technological requirements is investigated to propose first specifications answering these concerns. In the first section, the proposed process and rheological requirements for flow-based pultrusion are explained in the context of existing robotic extrusion strategies. The second section focuses on technology: the experimental apparatus for flow-based pultrusion is described, along with first experiments and proof of concept, validating the proposed theoretical framework. Finally, the effects of reinforcement ratio on process parameters as yield stress, pressure drops, or velocity effects are investigated to propose first specifications and first prescriptions for an operational and efficient flow-based pultrusion process.

2. Description of the flow-based pultrusion process

The flow-based pultrusion is an original process for extrusion-based additive manufacturing of continuously reinforced yield stress material. As well as existing pultrusion processes, it consists of impregnating continuous reinforcement fibers pulled through an extrusion die where the matrix, initially fluid to promote impregnation, is set to a hardened state, able to be extruded. The main difference is that pulling is not due to an external mechanism but to rheological properties of the yield stress material used as a matrix. Similarly to existing extrusion-based additive manufacturing processes, the extruded material is then

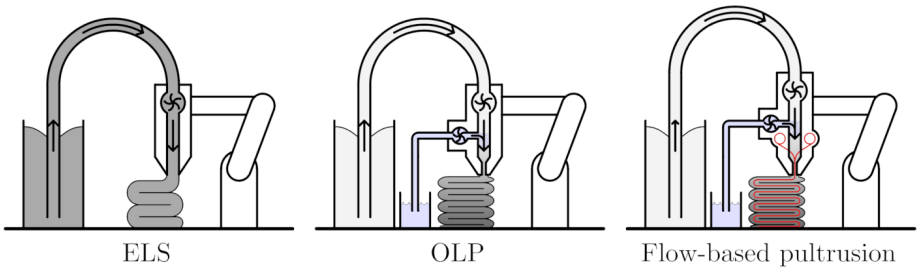

Figure 2: Schema comparing flow-based pultrusion to existing unreinforced additive manufacturing processes : Extrusion Lace Shaping (ELS) and Oriented Lace Pressing (OLP). Shades of grey indicates yield stress of the material.

spatially deposited by a robotic manipulator to shape the desired object. This complementary step yields notable requirements for the fresh material. Those will be reminded in the first section, with respect to existing strategies of unreinforced robotic extrusion processes. Finally, the adaptation of flow-based pultrusion to existing printing technologies is discussed.

2.1. Robotic extrusion of unreinforced cementitious materials, ELS and OLP strategies

The principle of robotic extrusion is to pump a yield stress material up to a printing head attached to a robotic manipulator, where it is extruded as a lace and spatially deposited. As described in [11], a material used for extrusion-based additive manufacturing must meet several rheological constraints with respect to the process steps. Indeed, it should be pumpable during extrusion, and able to self-support and support the weight of additional laces once deposited. Literature differentiates two strategies to meet these requirements [12], the key difference being the yield stress history of the material :

The simpler, single-phase *Extrusion Lace Shaping* (ELS) technology refers to processes where a lace of material, typically rectangular, is deposited layer by layer without pressing. The material exhibits a low but sufficient structuration rate (i.e. increase of material yield stress over time) and high yield stress (about 1000 Pa) from pumping to deposition, which are suitable to build-up several

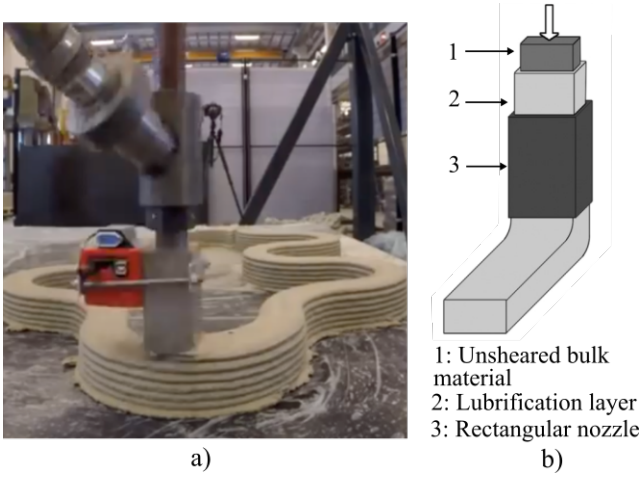

Figure 3: Robotic extrusion using Extrusion Lace Shaping : a) Picture of ELS extrusion (Extrusion technology of TU Eindhoven), b) Schema of the ELS extrusion [11]

layers at slow speed. In such conditions, a plug flow is imposed and material shearing should be limited to avoid destructuration of the extruded lace. Indeed, layers can't be pressed and nozzle orientation should stay tangential to the printing path. During extrusion, the lace section A_{lace} is prescribed by the nozzle shape. This yields a relation between the robot travel speed V_r and mortar mass flow rate Q :

$$Q = V_r A_{lace}$$

Unlike ELS, *Oriented-lace pressing* (OLP) is a two-phase approach with the addition of additives. The lace is shaped by pressing successive layers thanks to a lower extrusion yield stress. To meet buildability constraints, the viscosity or structuration ratio of the material can, respectively, be increased by the addition of a viscosity modifier agent (VMA) or accelerator just before extrusion. In this paper, only accelerator additives are considered. The initial material yield stress at the pumping stage is about 100 Pa, much lower than ELS. Nozzle orientation can remain constant, even for curve paths, and layer height is prescribed by the distance h between nozzle and previous layer. ρ being the concrete density, layer width w is given by the conservation of mass [13] :

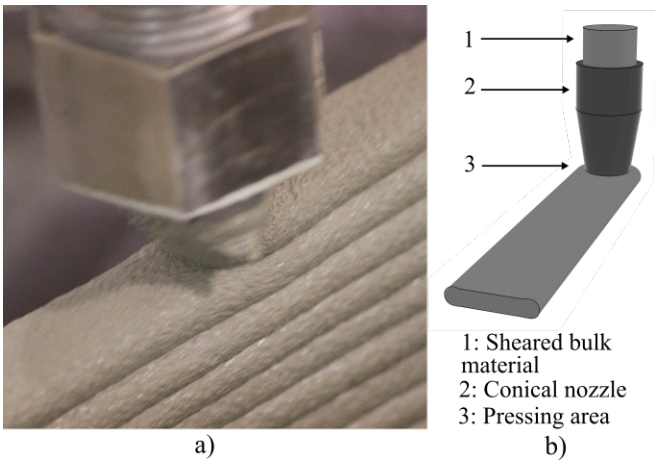

Figure 4: Robotic extrusion using Oriented Lace Pressing: a) Picture of OLP extrusion (Extrusion technology of Build in platform of Ecole des Ponts), b) Schematic of OLP (source : [10])

$$w = \frac{Q}{V_r h \rho}$$

2.2. From OLP to Flow-Based Pultrusion

The proposed flow-based pultrusion technology is very similar to OLP, the main difference being the addition of continuous reinforcements. A look at figure 6 gives a sense of the principle governing the process: After the addition of additives, continuous rovings are added at the location x_m where matrix yield stress is low, promoting impregnation. The higher yield stress in the reinforcement pulling zone of length l_p allows shear interaction between fiber and matrix, providing pulling force on rovings.

2.2.1. Kinematic requirements of flow-based pultrusion

As mentioned in [10], relative displacement is not allowed between reinforcement and matrix. Then, due to the rovings inextensibility, the area of the concrete lace after deposition should be equal to the one of the nozzle section. Consequently, the robot travel speed V_r must be equal to the flow velocity in

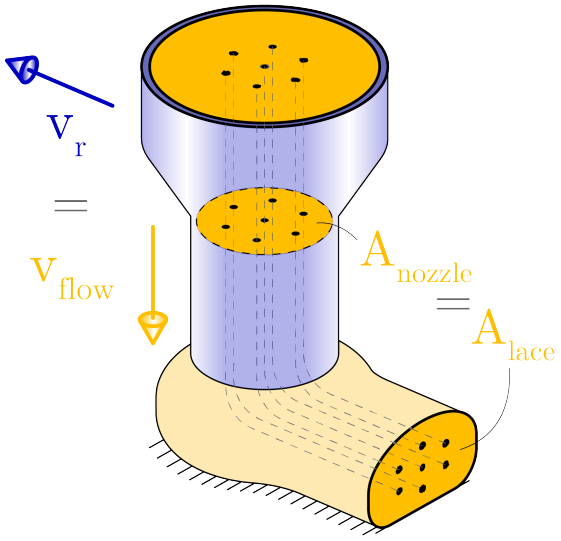

Figure 5: Schematic of the flow-based pultrusion nozzle (blue) and material flow (orange) during printing, where $A_{nozzle} = A_{lace}$ due to the inextensibility of the fibers (dashed lines). Consequently, V_r and V_{flow} should be equal.

the reinforcement pulling zone V_{flow}, which leads to the relation :

$$V_r = \frac{4Q}{\rho\pi d^2(1-\phi_f)} \tag{1}$$

Where d is the output diameter and ϕ_f the reinforcement roving ratio.

However, in practice, perfect equality is not achievable. The right term of equation (1) turns into the robot maximal admissible travel speed, before mismatch between roving and concrete speed. Besides, a smaller robot travel speed value yields to a wave pattern of fibers rovings, whose amplitude should remain sufficiently small.

2.3. Dynamic requirements for Flow-Based Pultrusion

In this paragraph we refer to some elements of a detailed analysis of the process requirements drawn in [10]. Using an asymptotic analysis of the generated pulling force on a continuous reinforcement roving with no relative displacement with the surrounding mortar, the maximal pulling force applied on each roving,

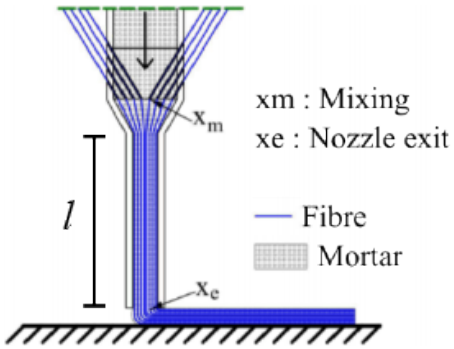

Figure 6: Schema of flow-based pultrusion [10]

noted F_{max}, is obtained by integration of the equilibrium equation of an element of the roving and is equal to :

$$F_{max} = \int_{x_m}^{x_e} \tau_c(x)\, p_r \, \mathrm{d}x \tag{2}$$

with p_r the cumulated perimeter of each fibers of the roving, x_e the location of nozzle exit and x_m the location of the rovings entry, defined in Figure 6. For a constant yield stress between mixing and nozzle exit, it gives :

$$F_{max} = \tau_c \, p_r \, l_p \tag{3}$$

with l_p the reinforcement pulling zone length (figure 6). The latter equation would make sense when using a constant high yield stress mortar, typical of ELS technology. Such mortar would provide good pulling force, but could lead to a lack of impregnation. Consequently, OLP technology seems more promising, as the initially low mortar yield stress would promote impregnation. The structuration ratio of such OLP mortar, which is accelerated by addition of additives, can be supposed linear with time as proposed in [14]. Therefore, an average pulling yield stress $\langle \tau_c \rangle$ is approximated from the input yield stress τ_{c0} and output yield stress τ_{ce} :

$$\langle \tau_c \rangle = \frac{\tau_{c0} + \tau_{ce}}{2} \tag{4}$$

It yields the F_{max} estimation for flow-based pultrusion :

$$F_{max} = \langle \tau_c \rangle \, p_r \, l_p \tag{5}$$

To ensure no relative displacement between roving and mortar during deposition, the maximal pulling force on one roving should be higher than the maximal frictional force experienced by the carried rovings from storage to the mixing point. Hence :

$$F_{max} \geq \max(F_{fr}^{i}) \tag{6}$$

3. Description of the proposed technology

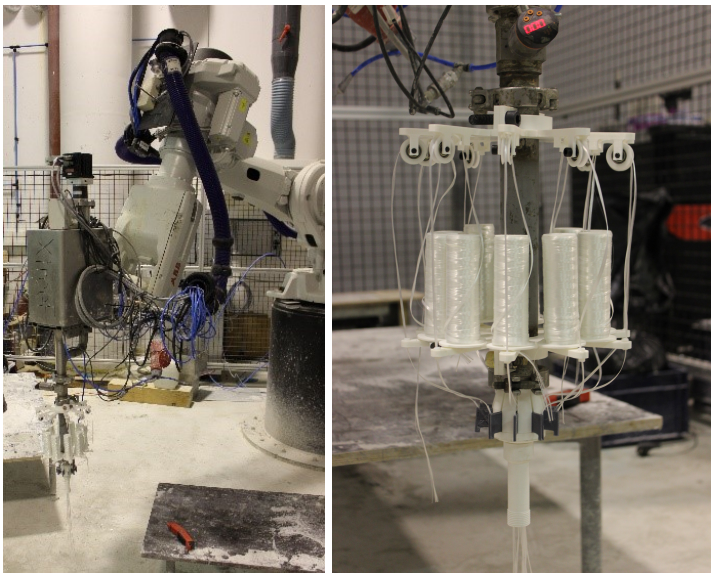

Figure 7: The flow-based pultrusion experimental device adapted on an XtreeE OLP concrete printing device of the Build'In robotic additive manufacturing cell.

The experimental setup relies on the *Build'In* robotic extrusion cell of the *Ecole des Ponts ParisTech* shown in figure 7. The novel flow-based pultrusion device adds up to an XtreeE OLP printing head carried by an ABB IRB 6620 industrial robot arm. The existing unreinforced extrusion nozzle of the printing

head is replaced with a flow-based pultrusion one. Two plates attached to the printing head carry 10 roving rolls and convey rovings up to the nozzle.

The setup is intended for validation of the process and producing prototypes as large as one cubic meter in size, with a reinforcement ratio up to 2%.

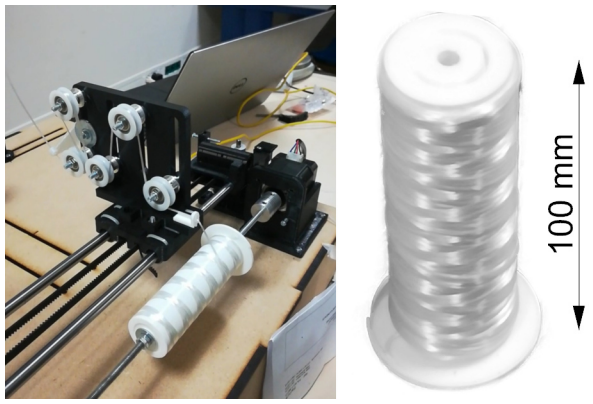

Figure 8: Picture of the rewinding device and roving package obtained.

3.1. Roving packages

It is notable that small roving packages are impossible to find due to the lack of industrial applications. Small bobbins of 100x45mm holding 30 meters of roving are rewound from standard bobbins using a custom apparatus shown in figure 8 and allowing a very controlled roll-up, avoiding knots and minimizing frictions. Experiments have been led using Isomatex Filava Conventional Multi-End 400 tex basalt rovings, AGY SCG75 and NEG AR310S800 AR glass rovings, whose properties are listed in table 2. The packaged roving length yields the maximum length of the printing path.

3.2. Roving conveying

The roving conveying system illustrated in figure 9 consists of two PLA 3D-printed platforms fixed on the printing head. Bobbins are fixed on the upper platform and rovings vertically unrolled. Rovings are conveyed through PTFE pinholes (1,3), pulleys (2), and inserted in the matrix through a PTFE tube (4).

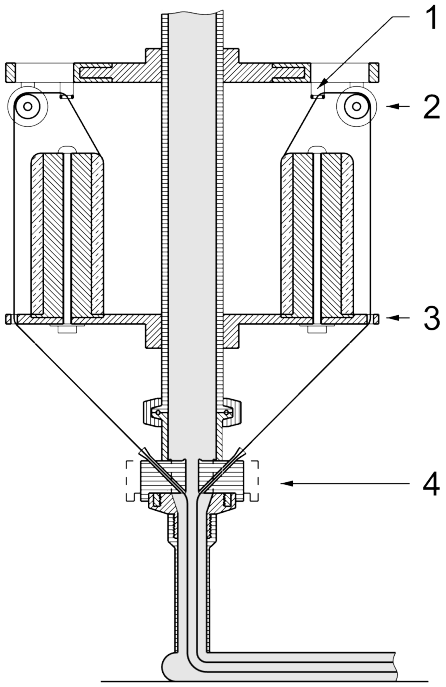

Figure 9: Section of the experimental device. (1), (3) : pinholes, (2) : pulley, (4) insertion tube.

3.3. Fiber impregnation, pulling and extrusion

Rovings are impregnated and pulled by the mortar in a flow-based pultrusion (FBP) nozzle replacing the existing extrusion nozzle of the XtreeE OLP printing head. The reinforcement pulling zone length l_p and output diameter d can be adapted to the process requirements thanks to a modular pulling area design with screw-in elements (5). Typical values are 10 - 18 mm for output diameter and 60 - 100 mm for pulling length.

4. Proof of concept

As a first experiment, three oblong hollow blocks are printed with different layer heights (6, 8, 10mm). The dimensions are 40x20x5cm. The Navier printable mortar (for reference composition see table 1) was used with NEG AR310S800 rovings.

Figure 10: 3d printing of anisotropic concrete.

Ingredient	Mass proportion
Cement	0.28
Water	0.11
Sand	0.44
Silica fume	0.16
Superplasticizer	0.003

Table 1: Reference composition of the Navier printing mortar.

4.1. Initial measurements and setting of parameters

In order to fulfill process requirements (see section 2), several process parameters are measured and/or tuned :

- Friction of each roving Fi_{fr} is measured by adding weights to the roving end until it is pulled.
- Mortar input yield stress τ_{c0} is measured with a slump test [15].

- Knowing τ_{c0}, Fi_{fr} and l_p, the required value for $\langle\tau_c\rangle$ is calculated and dosing of additives is tuned to obtain the right output yield stress τ_{ce} value measured with the slug test [16]. For practical reasons, the material is flowed through a specific flow test nozzle, having the same shape as the FBP one but no roving entries.

- The mortar mass flow rate Q is set to define robot travel speed V_r accordingly to eq. 1.

4.2. Starting up the process

Successfully immersing fibers in the first transient mortar flow is of utmost importance. Indeed, the initialization process needs special attention. A successful method is described now. After the latter measurement steps, the additive flow is stopped and mortar extrusion is visually inspected to check the yield stress resulting reduction. Once a low yield stress is reached (additive effect has disappeared), mortar pumping is temporarily stopped. The specific flow test nozzle is replaced with the real one, and rovings are manually inserted. Mortar pumping is then relaunched, and additives are progressively added so that the first transient flow has low yield stress and static rovings are properly impregnated. Finally, rovings start being pulled by mortar once sufficient yield stress is reached: the process is started.

4.3. First experimental results

The first experiments are shown in figure 10, the output diameter is 18mm, and the resulting reinforcement ratio is 0.2%. The global good aspect shows that the system works.

We have not noticed any cracking of the reinforced hardened laces. The fiber ratio is still low and we dry the specimens very slowly (during several days), and this permits a redistribution of internal pre-stresses due to shrinkage. Another reason is the low compressive stiffness of the reinforcements (rovings) we used for reinforcement. Shrinkage may lead to the buckling of rovings instead of the

matrix cracking. These first results, obtained with this first laboratory prototype, confirm the rheological analysis and the flow-based pultrusion strategy. [6]

5. Specifications of flow-based pultrusion : impact of process and technological requirements on reinforcement ratio

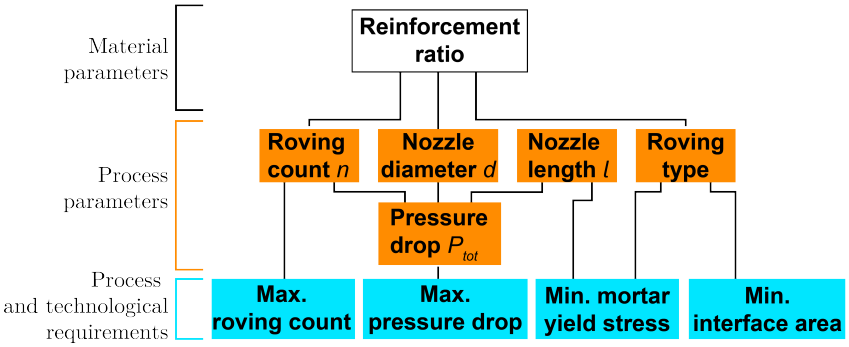

Figure 11: Flow chart summarizing the relation between reinforcement ratio as a material parameter with process and technological requirements.

Reinforcement ratio, that is, the volume percentage of fiber reinforcement embedded in the entire volume of a fiber-reinforced composite material is an important parameter controlling material properties. For composite materials, a higher reinforcement ratio generally yields better material properties, such as modulus and strength. It is therefore of interest to understand the limits of flow-based pultrusion regarding this material parameter. Figure 11 shows how one would check for the feasibility of a given reinforcement ratio. It is related to several process parameters (roving count, output diameter, roving type) and various value combinations may be found. However, those are limited by process and technological requirements. This section investigates the impact of those requirements: dimensioning calculations are proposed to discuss achievable reinforcement ratios.

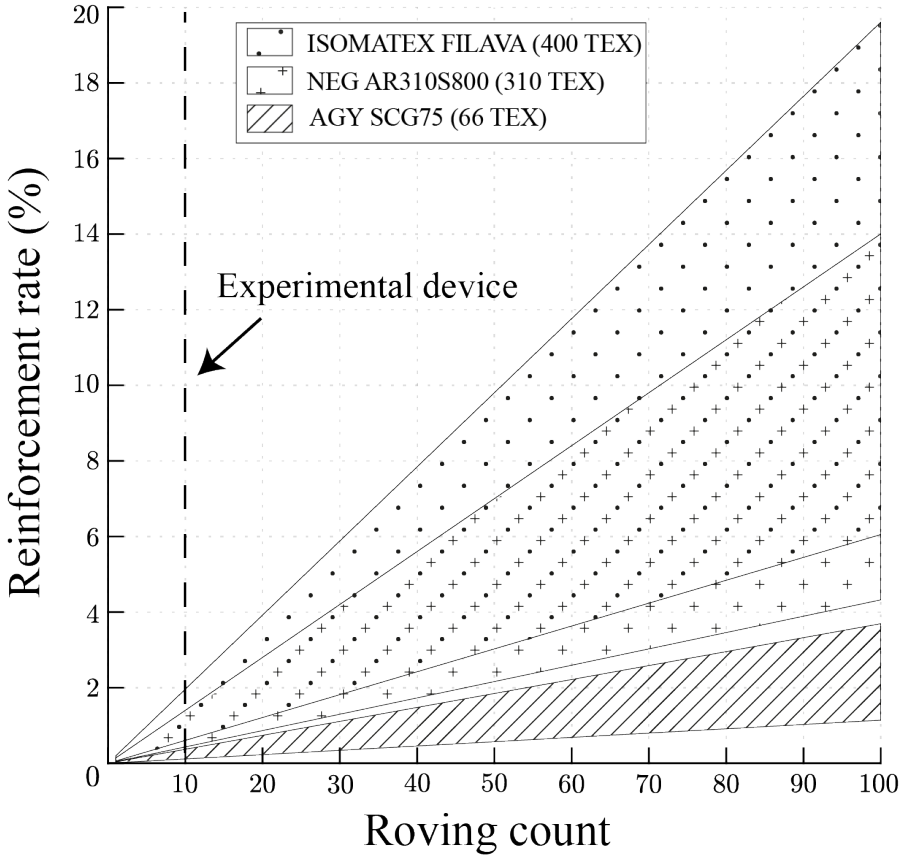

Figure 12: Graph of Reinforcement ratio (%) against roving count. For each roving type, hatched regions depict a range of achievable ratio depending on the output diameter, from 10 to 18mm.

Name	Material (-)	Titer (tex)	Density (g/cm^3)	A (mm^2)	f_{fil} (MPa)	E_{fil} (GPa)	ε_{max} (%)
AGY SCG75	AR glass	66	2,48	0,029	3570-3680	87-90	5,7
NEG AR310S800	AR glass	310	2,80	0,110	1500	74	2,0
Isomatex Filava	Basalt	400	2,61	0,154	3400-3700	88-94	2,4

A : Cross-section area of the filament; f_{fil} : tensile strength of the filament; E_{fil} : Tensile modulus of the filament; ε_{max} : ultimate strain.

Table 2: Characteristics of roving types tested for flow-based pultrusion.

5.1. Calculation of reinforcement ratio

The reinforcement ratio ϕ_f is the ratio between the cumulated rovings cross-section area and the extrusion cross-section area. Given a circular extrusion

nozzle, it yields:

$$\phi_f = \frac{4nA}{\pi d^2} \tag{7}$$

Where n is the roving count, A the unitary roving cross-section area, and d the output diameter. This equation shows that reinforcement ratio can be increased in several ways :

- Using rovings with a higher cross-section (i.e heavier rovings). Roving types tested for flow-based pultrusion are listed in table 2.
- Increasing roving count. Indeed, this roving count parameter is the hardest to play on in a laboratory setup, as it increases the apparatus complexity. Therefore industrial development seems essential to achieve the highest rates.
- Reducing output diameter. By using a 10mm output diameter, the 10-roving experimental device and the rovings with the highest cross-section (Isomatex Filava 400 tex), ratios up to 2% can be tested. The scale of objects produced by the current device, aiming at manufacturing thin-walled building components, leads us to consider a typical diameter range between 10-18mm.

Figure 12 shows the reinforcement ratio function of roving count for each roving type, with the lace diameter between 10 and 18mm. What can be clearly seen in this graph is the achievable ratios using the experimental device (allowing a maximum of 10 rovings) and with further technological development that would allow greater roving counts.

5.2. Reinforcement ratio and yield stress requirement

As explained in section 2.3, the mortar flow should be able to provide a sufficient force to pull the rovings. This force capacity F_{max} is dependent with the mortar mean yield shear stress $\langle \tau_c \rangle$, mean from mixing area to extrusion point, roving perimeter p_r and length of the reinforcement pulling zone l_p. If F_{max} is below the mean roving frictional force F_{fr}^i (eq.6), rovings are not pulled

and the process will likely fail. This condition (eq. 5) can be rewritten as a function of yield stress $\langle \tau_c \rangle$ and by detailing F_{max} as the expression $p_r \, l_p$ (eq. 5) :

$$\langle \tau_c \rangle \geq \frac{F_{fr}^i}{p_r \, l_p} \tag{8}$$

This gives the yield stress requirement for flow-based pultrusion. However, it should be kept in mind that yield stress requirements already exists in the context of OLP and concrete printing in general (see section 2.1). From a practical point of view, a rational strategy would be to start from the minimum yield stress required by the OLP process, and possibly increase it to meet the FBP condition. Still, if yield stress is increased, attention should be given to eventual cold joint effects between printed layers. More detail on how parameters are set in OLP can be found in [13].

5.2.1. Calculation of the yield stress requirement

Let us calculate a lower bound for the perimeter of a single roving p_r. Assuming the roving cross-section is circular, thus minimizing perimeter, the lower bound p_{min} is found from the roving cross-section area A :

$$p_r \geq p_{min} = 2\sqrt{\pi A} \tag{9}$$

This provides a conservative hypothese for the yield stress requirement equation 8, as substituting p_r with p_{min} yields the higher bound for $\langle \tau_c \rangle$.

F_{max} (eq.5) is then computed for a range of $\langle \tau_c \rangle$ values typical of the OLP process (300 To 800 Pa), different roving types with their respective perimeters p_r, and varying lengths of the reinforcement pulling zone l_p ranging from 50 to 150mm. This result is compared to the experimental value of the friction force F_{fr}^i (0.08 N) obtained with the device presented in section 3.

5.2.2. Discussion

Figure 13 depicts the calculated F_{max} values against mortar yield stress $\langle \tau_c \rangle$. It shows that using the heaviest rovings (NEG AR310S800 or ISOMATEX FILAVA 400TEX) does not raise concerns in most cases, except under 500 Pa

with low reinforcement pulling zone lengths. Oppositely, using the lighter AGY SCG75 roving (66 tex) is more constraining: High yield stress setting (600-800 Pa) and high pulling length are required.

Finally, this leads to the rather counter-intuitive conclusion that increasing the reinforcement ratio would either decrease or have no effect on the yield stress requirement:

- Increasing the reinforcement ratio by using heavier rovings yields a greater roving perimeter. Thus, other things being equal, the roving boundary surface exposed to mortar is larger, decreasing the yield stress requirement.
- Increasing the reinforcement ratio by reducing the output diameter or increasing roving count would not affect on this requirement, as the criterion applies to a single roving.

5.3. Reinforcement ratio and spacing between rovings

At the scale of the extruded section, which is reinforced with multiple rovings, the spacing between rovings should be considered for two reasons :

- To make sure that each fiber is surrounded by a volume of mortar providing impregnation and shear transfer.
- To allow the largest mortar grains to flow through the extruded section. Here, an absolute spacing criterion value can be defined, depending on the maximum grain size exhibited by the mortar granular skeleton.

5.3.1. Example of an extruded section with increasing roving count

To illustrate the purpose, Figure 14 shows an idealized drawing of a 10mm extruded section reinforced with Isomatex rovings. The reinforcement ratio is gradually increased from 10 to 20% by increasing roving count n. A consistent spacing distance, equivalent to the roving radius and about the average grain size of typical fine-grain sand (0.24mm) is maintained around rovings. The resulting spacing area is highlighted in red. The depicted roving arrangement does not

take into account the physical effects of extrusion and is only constrained by the spacing requirement.

- The 10% reinforced section shows sufficient space between rovings. In such a case, rovings can be considered independent.
- Increasing roving count up to a 15% reinforced section results in a denser arrangement, where the spacing criterion is still met.
- The 20% reinforced section approaches a density peak where no more rovings can be added while preserving consistent spacing. In such a case, it becomes insufficient to describe the yield stress requirement by a local criterion, as the mortar shear zones surrounding fibers may overlap. Moreover, it becomes evident that such a high reinforcement ratio would require the maximum grain size to be adapted.

In brief, considering a purely geometrical approach, this spacing criterion shows that reinforcement rates over 20% ultimately challenges the proposed theory, and call for the design of bespoke flow-based pultrusion mortars.

5.4. Reinforcement ratio effects on pressure drop

The flow-based pultrusion device adds up to an existing OLP printing device (See section 3) where the mortar is extruded by a pump regulating the mass flow rate. Indeed, increasing the pressure drop increases the pumping engine's work. If its capacity is exceeded, flow rate is not guaranteed and FBP requirements are not met (see the extrusion flow ratio-robot travel relation eq.1, section 2). A yield mechanism governs the flow of printed plastic mortars: once a critical shear stress τ_c is reached, mortar flows. In this section, a plasticity analysis is proposed to estimate the nozzle pressure drop P_{tot}, that is, the required pressure to initiate mortar flow in the FBP nozzle. The link between this process requirement and material reinforcement is investigated: Reinforcement ratio vs. Pressure drop estimations are given for the current device (see section 3) and future developments. Finally, results are compared with more restraining flow rate-dependence hypotheses.

5.4.1. Nozzle contribution to pressure drop

The flow-based pultrusion nozzle is a reducing pipe where pumping pressure should overcome shaping and frictional forces, like in a regular extrusion nozzle. Unlike regular nozzles, however, fibers are inserted and pulled by flow, which adds up to the total pressure requirement.

Let us detail shaping and frictional pressure drop contributions in the flow-based pultrusion nozzle :

- The shaping pressure P_{pl1} accounts for material strain in the reducing pipe section between mixing and pulling area,
- The wall friction P_{pl2} applying to mixing and pulling areas.

Material is supposed plastic and respecting the Tresca yield criterion, with elongational yield stress $\sigma = 2\,\tau_c$. Hence the ideal work equation for shaping a plastic material flow in a reducing circular pipe [17] yields the expression of P_{pl1}, with D and d being respectively input and output diameter :

$$P_{pl1} = \sigma\ \ln(\frac{D}{d}) \tag{10}$$

Supposing mortar exhibits a shear yield stress $\langle\tau_c\rangle$ in the reducing pipe (eq. 4) and according to the Tresca criterion, it yields :

$$P_{pl1} = 2\langle\tau_c\rangle\ \ln(\frac{D}{d}) \tag{11}$$

Replacing Tresca criterion with Von Mises criterion only implies that 2 in equation (11) should be replaced by $\sqrt{3}$. Using the Tresca criterion is then a conservative approach, appropriate for dimensioning purposes.

Considering a shear yield stress τ_c, and A being the cross-section area of the conduit and m its wall perimeter, the wall friction P_{pl2} can be defined according to force balance on a length l_p :

$$P_{pl2} = \tau_c\, l_p\, \frac{m}{A} \tag{12}$$

Assuming a circular conduit, it yields :

$$P_{pl2} = \tau_c \, \frac{4l_p}{d} \tag{13}$$

Yield stresses in mixing and pulling zone are respectively supposed equal to input yield stress τ_{c0} and $\langle \tau_c \rangle$. P_{pl2} is split in two contributions accounting for both zones with respective diameters D, d and lengths l_{mix}, l_p :

$$P_{pl2} = \tau_{c0} \, \frac{4l_m}{D} + \langle \tau_c \rangle \, \frac{4l_p}{d} \tag{14}$$

Hence the total shaping and frictional pressure drop contribution :

$$P_{pl} = P_{pl1} + P_{pl2} = 2\langle \tau_c \rangle \, \ln(\frac{D}{d}) + \tau_{c0} \, \frac{4l_m}{D} + \langle \tau_c \rangle \, \frac{4l_p}{d} \tag{15}$$

5.4.2. Fiber contribution to pressure drop

Fiber addition yields two contributions to the total pressure drop P_{tot} :

- Roving entries friction P_{mix} in the mixing area,
- The pressure P_{fr} needed to pull rovings.

The impregnation phase yields friction between the newly inserted fibers and the flowing mortar in the mixing zone. Considering a mixing area of a length l_{mix}, n being the roving count, τ_{c0} the input yield stress in the mixing area, and ϕ_f and d_f respectively the roving volumic ratio and diameter, P_{mix} is expressed according to force balance :

$$P_{mix} = \frac{4\tau_{c0} \, n \, \pi \, d_f \, l_{mix}}{(1-\phi_f)\pi \, D^2} \tag{16}$$

Due to the low perimeter of rovings d_f (about 0.5mm) and the low yield stress value at mixing point τ_{c0}, needed to enhance impregnation, this contribution has little impact and can be neglected.

P_{fr} is the sum of forces F^i_{fr} needed to pull n fibers, divided by the cross section area of the pulling zone :

$$P_{fr} = \frac{4nF^i_{fr}}{\pi d^2} \tag{17}$$

Quantity	Value
τ_{c0} (Pa)	200
τ_{ce} (Pa)	1000
$\langle\tau_c\rangle$ (Pa)	600
D (mm)	30
d_f (mm)	30
l_{mix} (mm)	50
l_p (mm)	50
F_{fr}^i (N)	0.08

Table 3: Typical values for the pressure drop estimation.

5.4.3. Discussion on pressure drop contributions

The later graph gives the pressure drop against output diameter for P_{fr} and $Ppl1 + Ppl2$ contributions. As P_{fr} is dependent with the roving count n, the P_{fr} range between 10 and 100 rovings is highlighted. Yield stress and nozzle geometry are set to typical values shown in table 3. For our experimental device (10 rovings, for 1-2% reinforcement ratio) the contribution of rovings on pressure drop is not significative but prescribed by shaping and frictional contributions. However, roving counts above 50 (allowing to reach $\phi_f \geq 10\%$) increase P_{fr} contribution which becomes predominant in the 10-15mm diameter range. A pressure drop about 0,3 to 0,6 bar for 50 rovings, and above 1 bar for 100 rovings, appears within this 10-15mm range, which is of specific interest for flow-based pultrusion as allowing to achieve the highest reinforcement rates. Pressure drop continues growing significantly for diameters smaller than 10mm, which seems unadapted to the process. Oppositely, considering the larger diameter range commonly used for unreinforced printing (15-20mm) the pressure drop is much less significative : the $P_{pl1} + P_{pl2}$ contribution converges to a plateau of 0.2 bar, and the pressure drop range of variable P_{fr} reduces from 0.6 bar (100 rovings, ø15mm) to values approaching zero.

5.4.4. Total pressure drop and application to the present setup

P_{mix} being negligible, the total pressure drop P_{tot} of flow-based pultrusion is the sum of P_{pl1}, P_{pl2} and P_{fr} contributions :

$$P_{tot} = P_{pl1} + P_{pl2} + P_{fr} = 2\langle\tau_c\rangle \ln(\frac{D}{d}) + \tau_{c0}\,\frac{4l_m}{D} + \langle\tau_c\rangle\,\frac{4l_p}{d} + \frac{4nF^i_{fr}}{\pi d^2} \quad (18)$$

To rely the calculations to our present setup, a pressure threshold accounting for its technological limitations is prescribed. As not to exceed the pump capacity, let us define a 1 bar threshold on the pressure drop due to the FBP device P_{tot}.

The graph 16 shows the total pressure drop P_{tot} against output diameter. For the existing device shown in section 3, the pressure drop curve for $n = 10$ rovings is under 1 bar. Indeed $n = 10$ is the maximum capacity of this device. Since this capacity will evolve with technological developments, considering higher n values gives a perspective view on the pressure drop limitation. For example, using the smallest output diameter (10mm, see section 5.1) the maximal roving count achievable below the 1 bar threshold is 55.

5.4.5. Achievable reinforcement ratios and specifications

Figure 17 gives an overview of achievable reinforcement ratios with respect to pressure drop, roving count and output diameter. Roving type is ISOMATEX Filava 400 Tex, so to maximize reinforcement ratio (see 5.1). Two ranges of output diameter stand out by their pressure drop levels and achievable rates. The range of typical output diameters for unreinforced printing (15-20mm) yields lower pressure drops and reinforcement ratios about 5% as a maximum. The smaller 10-15mm diameter range would allow 10% reinforcement rates but is more challenging from the process point of view as the pressure drop increases drastically. For example, 11% reinforcement ratio is obtained with 55 Isomatex rovings and a ø10mm nozzle. Looking forward, increasing the pressure drop threshold to 1.5 bar would allow 100 rovings and ratio about 20%.

5.5. Flow velocity effects on pressure drop

Moving beyond the requirements to initiate the flow, let us consider the process under steady-state flow conditions. The pressure drop is also flow-velocity-dependant and this must be investigated. Several approaches permit to estimate this effect, and Benbow and Bridgwater for instance proposed in [18] such a model. It derives from the plastic shaping (eq. 10) and friction (eq. 13) pressure drops with added velocity-dependent terms. Empirical parameters are obtained from paste extrusion tests where the input pressure is measured. Apparent elongational yield stress σ is split in two contributions: σ_0 the elongation yield stress when the velocity tends to zero, plus a term involving the flow velocity V and a fitting coefficient α. Similarly, the apparent wall shear stress is split in a wall shear yield stress τ_0, and a term function of flow velocity V and coefficient β. The new pressure drop expression, P_{BB} is, as follow:

$$P_{BB} = 2(\sigma_0 + \alpha V)\ln(\frac{D}{d}) + (\tau_0 + \beta V)\frac{4L}{d} \tag{19}$$

V depends on known process parameters : the pump-regulated mortar mass flow rate Q, mortar density ρ and output diameter d :

$$V = (Q/\rho)/((\pi\, d^2)/4) \tag{20}$$

In eq. 19, the relationship is supposed linear. However, the experiments rather highlight a non-linear influence of the flow velocity on the pressure drop. Hence a better fit may be found by using a six-parameters form of the Benbow-Bridgwater equation [19], where exponents n and m are introduced and have to be identified :

$$P_{BB} = 2(\sigma_0 + \alpha V^n)\ln(\frac{D}{d}) + (\tau_0 + \beta V^m)\frac{4L}{d} \tag{21}$$

This model has been successfully used to describe the extrusion behaviour of various pasty materials [19] [20]. Figueiredo et al. [21] provided the Benbow-Bridgwater equation parameters of a smooth mortar of consistency comparable

Name	α (KPa.s/mm)	β (KPa.s/mm)	σ_0 (KPa)	τ_0 (KPa)	m	n
YVA1	0,41	0,18	4,08	0,74	0,17	0,37

Table 4: Benbow-Bridgwater parameter values extracted from [21].

to a mortar as used in our application. Table 4 lists the parameter values of interest, extracted from [21].

A comparison between such velocity-dependant pressure drop estimation P_{BB} and P_{pl} (no velocity-dependency, equation 15) is given in figure 18 for different mass flow rate Q. Q and V are linked by eq. 20. For $Q = 0$ the two approaches are equivalent but P_{BB} pressure drop increases drastically, up to 1 bar for $d = 10$ mm and $Q = 50$ g/s.

This aspect has to be keep in mind for further industrial developments.

6. Conclusion

The technology and process specifications of a new reinforcement process applied to concrete 3D printing, called Flow-Based Pultrusion, have been presented. The ambition of the process is to provide an efficient reinforcement method for concrete additive manufacturing, able to reach high levels of reinforcement (2-10%) to obtain good mechanical properties. Main contributions are :

- The technical description of a first experimental apparatus for flow-based pultrusion, and a first experiment with 0.2% reinforcement ratio using 400 Tex Glass and Basalt rovings validating the theoretical framework and technology.
- The effects of reinforcement ratio on process parameters as yield stress, pressure drops or velocity effects are investigated to propose first specifications and first prescriptions for an operational and efficient flow based pultrusion process: ratios up to 2% seem achievable with the present setup

and rovings, and could ideally go up to 20% with further technological development.

Future works will continue to develop and improve the process, to investigate the potential of Flow-Based Pultrusion, and the new possibilities for the 3D printing process itself. Indeed the drastically increasing consistency of the fresh lace, even with few fibers (0,2%), permits a more easy handling and avoids avalanche and slug effects during the printing. Many new ways of printing are thinkable with such an intimately reinforced fresh lace, as cantilever or steep situations. Of course, the mechanical behaviour of the resulting anisotropic concrete is also studied. First tension and bending tests investigate the effects on ductility and ultimate strength. The first results show that the results depend highly on the mortar yield stress during the mixing. This parameter has a high influence on the interface quality between fibers and matrix and consequently, on the kind of shear transfer (stiff or soft) between them, as shown in previous studies [22]. This is of utmost interest for flow-based pultrusion, as yield stress is finely tunable anytime through the addition of additives. Confirmation of these results would open avenues towards novel additive manufacturing optimization strategies, by providing not only bespoke geometry but also bespoke material properties.

7. Acknowledgements

This work was funded by Labex MMCD (MultiScale Modelling and Experimentation of Materials for Sustainable Construction), which benefits from French government grants managed by the French National Research Agency ANR within the frame of the national program Investments for the Future (grant no. ANR-11-LABX-022-01), and by Ecole des Ponts ParisTech and its technological platform Build'in which benefits from Région Ile-de-France financial support (SESAME PIA3) . The authors also acknowledge the fruitful collaboration with XTreeE, technology provider of the extruder and HAL Robotics for joined software development for robotic control.

References

[1] D. Asprone, C. Menna, F. P. Bos, T. A. M. Salet, J. Mata-Falcón, W. Kaufmann, Rethinking reinforcement for digital fabrication with concrete, Cement and Concrete Research 112 (2018) 111–121. doi:10.1016/j.cemconres.2018.05.020.

[2] S. Lim, R. A. Buswell, T. T. Le, S. A. Austin, A. G. F. Gibb, T. Thorpe, Developments in construction-scale additive manufacturing processes, Automation in Construction 21 (2012) 262–268. doi:10.1016/j.autcon.2011.06.010.

[3] G. Vantyghem, W. De Corte, E. Shakour, O. Amir, 3D printing of a post-tensioned concrete girder designed by topology optimization, Automation in Construction 112 (2020) 103084. doi:10.1016/j.autcon.2020.103084.

[4] F. P. Bos, Z. Y. Ahmed, E. R. Jutinov, T. A. M. Salet, Experimental Exploration of Metal Cable as Reinforcement in 3D Printed Concrete, Materials (Basel, Switzerland) 10 (11) (Nov. 2017). doi:10.3390/ma10111314.

[5] T. Marchment, J. Sanjayan, Mesh reinforcing method for 3D Concrete Printing, Automation in Construction 109 (2020) 102992. doi:10.1016/j.autcon.2019.102992.

[6] V. Mechtcherine, A. Michel, M. Liebscher, T. Schmeier, Extrusion-based additive manufacturing with carbon reinforced concrete: Concept and feasibility study, Materials 2020 13 (2020) 2568. doi:10.3390/ma13112568.

[7] M. Hambach, Portland cement paste with aligned carbon fibers exhibiting exceptionally high flexural strength ($>$ 100MPa), Cement and Concrete Research (2016) 7.

[8] B. Zhu, J. Pan, B. Nematollahi, Z. Zhou, Y. Zhang, J. Sanjayan, Development of 3D printable engineered cementitious composites with ultra-high tensile ductility for digital construction, Materials & Design 181 (2019) 108088. doi:10.1016/j.matdes.2019.108088.

[9] R. Matsuzaki, M. Ueda, M. e. a. Namiki, Three-dimensional printing of continuous-fiber composites by in-nozzle impregnation, Scientific Report 6 (2016). doi:10.1038/srep23058.

[10] N. Ducoulombier, L. Demont, C. Chateau, M. Bornert, J. Caron, Additive manufacturing of anisotropic concrete – a flow-based pultrusion of continuous fibers in a cementitious matrix., Procedia Manufacturing 47 (2020) 1070–1077. doi:10.1016/j.promfg.2020.04.117.

[11] N. P. Roussel, Rheological requirements for printable concretes, 2018. doi:10.1016/j.cemconres.2018.04.005.

[12] R. Duballet, Systèmes constructifs en fabrication additive de matériaux cimentaires, Ph.D. thesis (Sep. 2019).

[13] P. Carneau, R. Mesnil, N. Roussel, O. Baverel, Additive manufacturing of cantilever - from masonry to concrete 3d printing, Automation in Construction (2020).

[14] R. N., A thixotropy model for fresh fluid concretes: Theory, validation and applications, Cement and Concrete Research 36 (2016) 1797–806. doi:https://doi:10.1016/j.cemconres.2006.05.025.

[15] N. Roussel, P. Coussot, "Fifty-cent rheometer" for yield stress measurements: From slump to spreading flow, Journal of Rheology 49 (May 2005). doi:10.1122/1.1879041.

[16] N. Ducoulombier, P. Carneau, R. Mesnil, J.-F. Caron, N. Roussel, "the slug test": Inline assessment of yield stress for ex-trusion-based additive manufacturing, in: Second RILEM International Conference on Concrete and Digital Fabrication – Digital Concrete 2020, 2020.

[17] C. R. Calladine, Plasticity for Engineers: Theory and Applications, reprint Edition, Ellis Horwood Series in Engineering Science, Horwood [u.a.], Chichester, 2000, oCLC: 816471643.

[18] J. J. Benbow, E. W. Oxley, J. Bridgwater, The extrusion mechanics of pastes—the influence of paste formulation on extrusion parameters, Chemical Engineering Science 42 (9) (1987) 2151–2162. doi:10.1016/0009-2509(87)85036-4.

[19] J. J. Benbow, S. H. Jazayeri, J. Bridgwater, The flow of pastes through dies of complicated geometry, Powder Technology 65 (1) (1991) 393–401. doi:10.1016/0032-5910(91)80201-S.

[20] X. Zhou, Z. Li, Characterization of rheology of fresh fiber reinforced cementitious composites through ram extrusion, Materials and Structures 38 (1) (2005) 17–24. doi:10.1007/BF02480570.

[21] S. Chaves Figueiredo, C. Romero Rodríguez, Z. Y. Ahmed, D. H. Bos, Y. Xu, T. M. Salet, O. Çopuroğlu, E. Schlangen, F. P. Bos, An approach to develop printable strain hardening cementitious composites, Materials & Design 169 (2019) 107651. doi:10.1016/j.matdes.2019.107651.

[22] N. Ducoulombier, C. Chateau, M. Bornert, J.-F. Caron, P. Aimedieu, T. Weitkamp, J. Perrin, A. King, M. Scheel, X-ray tomographic observations of microcracking patterns in fibre-reinforced mortar during tension stiffening tests, Strain (2020) e12347doi:10.1111/str.12347.
URL http://doi.wiley.com/10.1111/str.12347

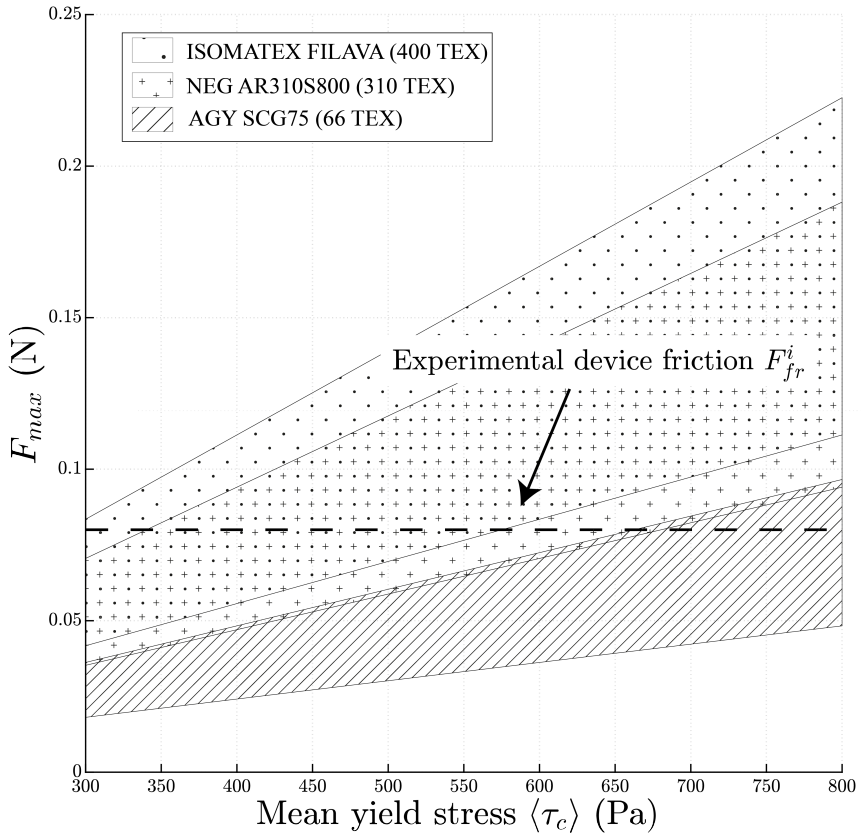

Figure 13: Graph of F_{max} against $\langle \tau_c \rangle$. For each roving type, hatched regions depict the F_{max} range depending on reinforcement pulling zone length l_p, ranging from 100 to 200mm. As F_{max} should be greater than F_{fr}^i to allow FBP, the experimental value of F_{fr}^i is shown for comparison.

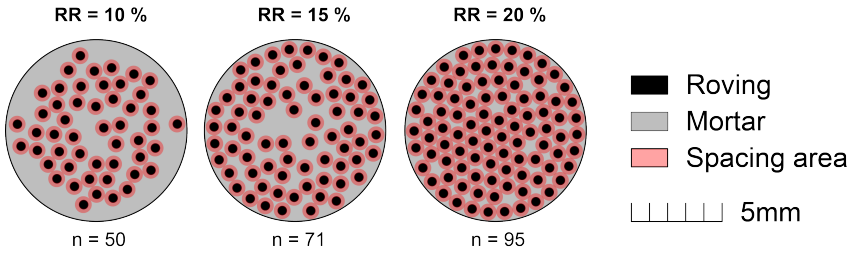

Figure 14: Schematic of a 10mm diameter extruded lace with different reinforcement ratios (RR) using Isomatex Filava 400 tex rovings (0.46mm diameter) and varying roving count (n). In order to allow flow-based pultrusion, rovings need to be surrounded with mortar providing shear transfer.

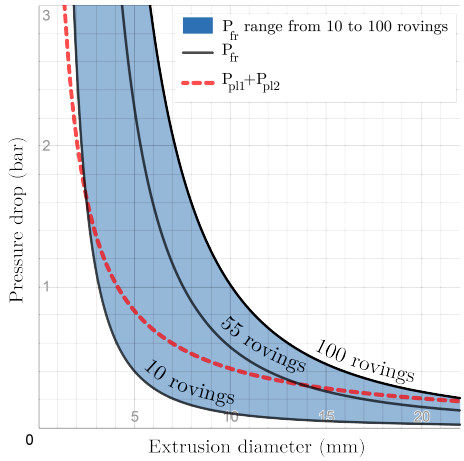

Figure 15: Pressure drop contributions (bar) of P_{fr} and P_{pl1}+P_{pl2} against output diameter (mm) for 10 to 100 rovings.

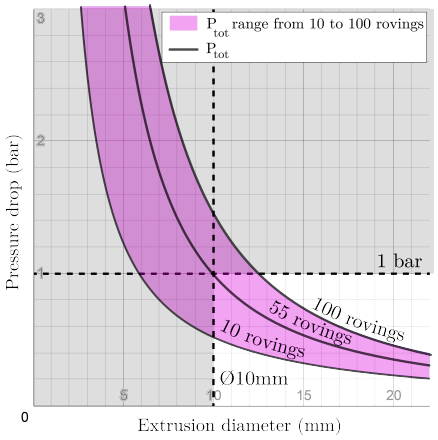

Figure 16: Total pressure drop P_{tot} against output diameter (mm) for 10 to 100 rovings. The maximum achievable roving count of 55 rovings using a ø10mm nozzle and pressure threshold of 1 bar is highlighted.

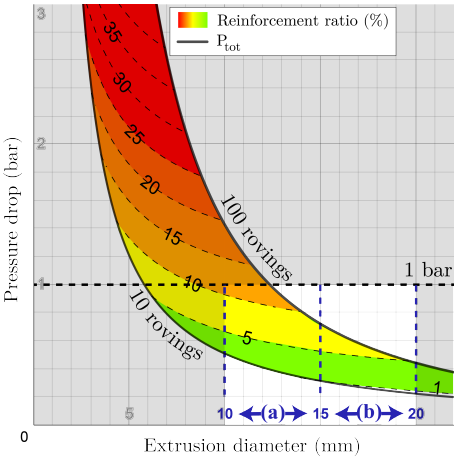

Figure 17: Map of achievable reinforcement ratios within a range of 10 to 100 rovings, against pressure drop and output diameter.

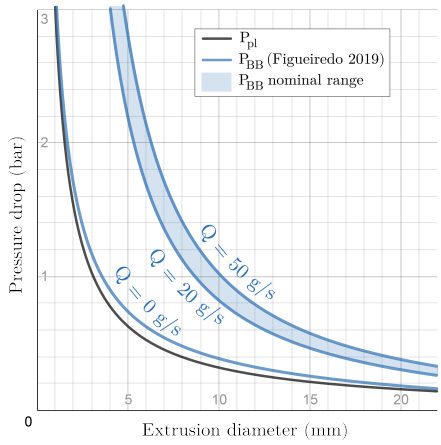

Figure 18: Pressure drop against output diameter for the velocity-independent case P_{Pl} and the velocity-dependant one P_{BB}. Parameter values from table 4, extracted from [21]. Flow rates between 20 and 50 g/s, $l_p = 100$mm.